Shock Events in the Solar System: The Message from Minerals in Terrestrial Planets and Asteroids

Philippe Gillet[1] and Ahmed El Goresy[2]

[1]Institute of Condensed Matter Physics, École Polytechnique Fédérale de Lausanne, 1015 Lausanne, Switzerland; email: philippe.gillet@epfl.ch

[2]Bayerisches Geoinstitut, Universität Bayreuth, 95447 Bayreuth, Germany; email: ahmed.elgoresy@uni-bayreuth.de

Annu. Rev. Earth Planet. Sci. 2013. 41:257–85

First published online as a Review in Advance on March 7, 2013

The *Annual Review of Earth and Planetary Sciences* is online at earth.annualreviews.org

This article's doi: 10.1146/annurev-earth-042711-105538

Keywords

impacts, high pressure, meteorites, craters, melt pockets, shear melt veins

Abstract

Impacts are central to the origin and evolution of planets of the Solar System. The shapes of craters, which can reach up to 1,000 km in diameter on the Moon, provide critical information on the large-scale dynamics of the impact and related shock. Minerals formed at high pressure and temperature found in shocked terrestrial rocks and meteorites give additional and complementary insights on the shock process at a smaller scale, typically from a few micrometers to a few millimeters. Local flaws in rocks, such as voids and mineral interfaces, are the preferential sites for the formation of high-pressure melts and minerals. Calculations based on the physics of shocks and the thermodynamics and kinetics of mineral transformations provide orders of magnitude for the duration, transient pressure, and prevailing temperature conditions of shock events. Case studies on shocked terrestrial and extraterrestrial materials illustrate the links between these parameters and impact duration. Many of the high-pressure mineral phases of olivine, pyroxenes, feldspars, silica, phosphates, titanium oxide, and carbon have been discovered in these heavily shocked rocks and provide unique opportunities to study the high-pressure minerals that exist in the deep Earth.

INTRODUCTION

The physics of high-velocity impacts and shocks is of fundamental interest to Earth and planetary sciences as well as to material science, industry, and defense. Shocks are involved in the birth, evolution, and destruction of planets in all planetary systems, including the Solar System. Impacts continue to shape the faces of Earth and other planetary bodies. The study of these collisions and the rocks and meteorites they produce has driven major discoveries in impact dynamics and high-pressure physics, chemistry, and mineralogy.

Since the birth of the Solar System, some 4.57 billion years ago (Gya), collisions and shocks have been essential actors in the formation and evolution of the planets (Montmerle et al. 2006, Morbidelli et al. 2012). At the beginning, the settling of dust onto the equatorial disk of the solar nebula and the formation of kilometer-sized planetesimals took place by a collision/accretion process. This initial stage was followed by the runaway growth of planetesimals to form Mars-sized planetary embryos, and finally by collisions of planetary embryos to form the planets through oligarchic growth. These gigantic collisions released sufficient energy to cause large-scale melting, the formation of magmatic oceans several hundreds of kilometers deep, and magmatic differentiation of the terrestrial planets (Elkins-Tanton 2012). Geochemical evidence and numerical modeling have demonstrated that the Moon resulted from the collision between the proto-Earth and a Mars-sized planetesimal some 30–50 Ma after the crystallization of the first minerals from the solar nebula (Canup & Asphaug 2001, Jacobsen 2005). Some 60 Ma later, asteroids and/or comets, rich in volatile compounds and organic matter and originating mostly from the outermost parts of the Solar System, might have hit Earth and contributed to the formation of the terrestrial ocean (Albarede 2009).

The history of large collision events is recorded in craters on the surfaces of planets (**Figure 1**) (Strom et al. 2005). The impact record is better preserved on planets and satellites with limited internal activity and no atmosphere or ocean, such as Mercury, the Moon, and the various asteroids and comets. The number of collisions in our Solar System was initially high, and most of the gigantic ones took place in the first hundred million years after its birth. Evidence suggests that after a rather quiet period, a heavy bombardment took place some 3.9 Gya as a result of a large flux of asteroids and comets that came from the outermost parts of the Solar System and crossed the orbits of the major planets, especially Earth (Bottke et al. 2012). This late bombardment may have affected both the internal and external activity of the young Earth and Mars. Given this history and using the calibrated cratering curve of the Moon, impact crater densities and crater size distribution can be used to provide the ages of planetary surfaces and/or the timing of changes in colliding asteroid fluxes (Bottke et al. 2012, Hartmann 2002). The age distribution of craters on the Moon can thus be used as a proxy for estimating the impact history of geologically active bodies such as Earth.

Gigantic impacts affect internal planetary dynamics through large-scale melting. During a shock on Earth's surface, large volumes of melt are directly produced at the impact point. Moreover, the deformation at depth associated with the crater can induce partial melting in Earth's mantle. Some authors have proposed that some of the large igneous provinces (LIPs) found on Earth (continental flood basalt provinces, volcanic rifted margins, and giant oceanic plateaus) might have been triggered by large impacts (Jones et al. 2002). The time correlation between impacts and LIPs remains troubling and controversial, especially when massive species extinctions are involved. The Tunguska event in Siberia at the beginning of the twentieth century reminded us of the actual risk of Earth colliding with comets or asteroids (Chyba et al. 1993).

Asteroid impacts occurring after the beginning of life on Earth (4.4–4 Gya) also had an important influence on the evolution of life (Reimold & Jourdan 2012). For instance, asteroid impacts probably triggered large global biological species extinctions several times throughout the history

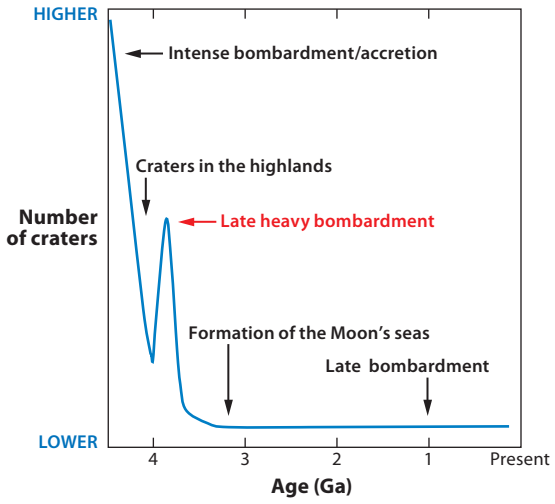

Figure 1

A schematic curve showing the decrease of the number of impacts recorded on the planetary surfaces of the Solar System. At the beginning of the Solar System, the number of impacts was very high. The intermediate peak near 3.9 Gya is often termed the late heavy bombardment.

of Earth; the most popular one occurred at the Cretaceous-Tertiary boundary, some 65 Mya, putting an end to the era of dinosaurs. The collision between a 10-km-sized asteroid and Earth can inject into the atmosphere large amounts of ashes, water, and CO_2, which can remain there for centuries, significantly altering Earth's climate and thus its planetary ecosystems (Pierazzo & Artemieva 2012).

The history of impacts can be quantified at various scales and with different tools. A first approach consists in studying the morphology and size of craters formed during the shocks. A second approach, when samples are available, is to characterize the deformations and transformations induced in rocks and minerals during the transient pressure and temperature changes. This approach can also be reversed: Micro- and macroscale analysis of impact craters reveals the physics of planetary accretion and the material response of multiphase systems to shocks.

Studying and dating the crater record on the Moon have been an essential step for proposing collision/accretion models for planetary formation. The crater distribution on the Moon reveals that among the thousands of recognized craters, 1,700 exceed 20 km in diameter, and 15 range between 300 and 1,200 km in diameter (Stöffler et al. 2006). Because of its greater size, Earth has received a higher flux of asteroids through time: 22,000 craters exceed 20 km in diameter, and between 40 and 200 exceed 1,000 km in diameter. However, most of the craters, especially the older ones, have been erased by plate tectonics, which completely renews a large part of the planet's (oceanic) surface every 200 Ma. On the continents, erosion, weathering, and sedimentation have also played major roles in erasing and masking the relief of craters.

Only a few places on Earth allow the complete study from crater morphology to ejecta, rock records, and mineralogical changes (Jourdan et al. 2012). The shock histories of these localities can be addressed in detail through the study of the dynamically deformed rocks and shock melts within the terrain of individual impact craters. However, such a study is promising mainly for craters excavated in impact events in the past several hundred million years—e.g., Ries in Germany, Barringer in the United States, and Popigai in Russia—whose ejecta were not subjected

to late metamorphic overprinting. Shocked meteorites, depending on their origin, also provide an important source of information for understanding the dynamics of impacts at different stages of the evolution of the Solar System.

In some cases, evidence of former collisions can be found in sedimentary records or ice cores in the form of spherule layers (Johnson & Melosh 2012). In fact, during the initial stage of a shock, when an asteroid first comes into contact with Earth's surface, jets of molten crustal materials can occur that account for most of the tektites and glassy spherules observed in sedimentary rocks deposited at the time of the impact (Bottke et al. 2012, Housen & Holsapple 2011).

A second way to quantify shocks consists in the study of the deformations and transformations induced in rocks and minerals by the transient pressure and temperature changes. This so-called shock metamorphism induces various modifications in the impactor and the impacted rocks: (*a*) fracturing, (*b*) plastic deformation, (*c*) amorphization of solids, (*d*) polymorphic phase transitions, and (*e*) melting and vaporization.

Recent impacts on the Moon, Mars, and asteroids such as Vesta are responsible for the ejection into space of rock fragments, which, after falling on Earth, provide us with valuable information to study the surfaces and internal processes of these planetary bodies (Barrat et al. 2002, Marchi et al. 2012, Treiman et al. 2000, Warren et al. 2005). These heavily shocked meteorites and chondrites (primitive meteorites that are 4.56 Ga old) represent a unique opportunity for studying deformations and phase transitions that resulted from recent impact events in the Solar System.

In this article, we focus on the mineralogical transformations associated with a shock event on planetary materials. We first give a short overview of the physics of shocks using basic equations; of the orders of magnitude of the pressure and temperature changes; and of how those parameters relate to the impact's macroscopic parameters such as the velocity and size of the impactor. We then use these results to explore the related transformations that occur in some of the major rock-forming minerals. The study of impact metamorphism on rocks and minerals also provides valuable information on the phase transformations that can occur during subduction of terrestrial rocks and on the mineralogy of the deep Earth (Gillet et al. 2007).

THE TIMESCALE OF NATURAL SHOCKS

Although the record of a collision could last for eons, collisions are violent and short phenomena. A few typical orders of magnitude can be put forward. The relative velocity of asteroids in the asteroid belt is on the order of 5 km s^{-1}. The median impact velocity on Earth is approximately 18 km s^{-1}. On Mars, this speed is on the order of 10 km s^{-1}. Depending on the size of the impacting asteroid, the shock duration can range from a few tens of milliseconds to a few seconds. Pressure can exceed 100 GPa and temperature can reach 10,000 K, enough to induce melting and vaporization of rocks. The energy released in an impact caused by a 300-m-diameter impactor is on the order of 4×10^{18} J.

Many review papers or books can be consulted for a detailed overview of such an event (see, e.g., Collins et al. 2012, Melosh 1989). **Figure 2** shows the three stages used for describing the formation and evolution of a crater. The first stage, when the asteroid hits the surface and penetrates into the planet crust, is usually referred as the contact and compression phase. During this phase, the kinetic energy is transferred through the contact zone to both the target and impactor, inducing in both of them a strong compression that leads to the creation, propagation, and spherical spreading of shock waves.

Owing to the dramatic induced pressure and temperature changes, the rocks are compressed and can even melt or vaporize. Molten material often squirts out and is projected far away from the impact point. The duration, τ, of the shock is roughly the time required for the projectile to

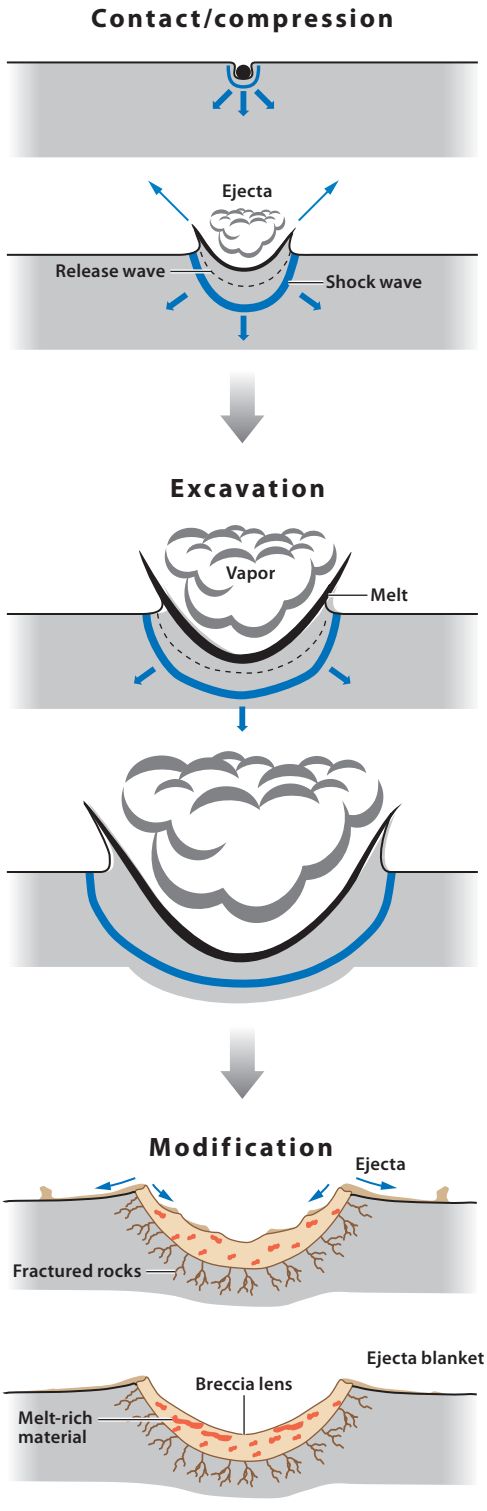

Figure 2

Schematic phenomenological model for the formation of an impact crater and ejecta deposits. Adapted from French (1998).

Table 1 Typical crater sizes observed on asteroids[a]

Asteroid	Crater size (m)	Impactor size (m)	Shock duration (s)
Vesta	400×10^3	24×10^3	4.8
Mathilde	30×10^3	310	6×10^{-2}
Gaspra	500	2.4	4×10^{-4}

[a]Impactor sizes and shock durations are derived from Equations (1) and (2). The collision speed is fixed to 5 km s^{-1}.

travel within the target a distance equal to its diameter d. For a given speed v_i, this time is

$$\tau = \frac{d}{v_i}. \quad (1)$$

The next stage, excavation, corresponds to the ejection of material from the expanding cavity in the form of vapor, melt and solid blocks, and dust. The ejected material falls back, forming an ejecta blanket in and around the crater. This stage can last from a few seconds to a few minutes. The final stage is called modification and results in the collapse of the crater due to gravity.

The size of the transient crater can be evaluated through several scaling laws (Melosh 1989). They relate the crater diameter, D_c, to the target density (ρ_t), the impactor density (ρ_i), the impactor diameter (d), the impactor kinetic energy (W_t), the angle of the collision, and the target surface gravity (g). For the special case of a vertical impact, a classical scaling law is provided by the following equation:

$$D_c = 1.8 \times \rho_i^{0.11} \times \rho_t^{0.33} \times g^{-0.22} \times d^{0.13} \times W_t^{0.22}. \quad (2)$$

Other scaling laws that take into account the angle of collision can be found in the literature (Collins et al. 2005). Using Equations (1) and (2), one can compute the expected crater size as a function of the impactor speed for various shock durations, or vice versa (**Table 1**).

By comparison, laboratory shock recovery experiments have a typical effective duration of approximately a microsecond. This short timescale results from the typical speed of the impactor (10 km s^{-1}) and the characteristic size of the projectile (1 cm). The several orders of magnitude difference in the shock duration can lead to major differences between experimentally produced mineral changes and those observed in naturally shocked rocks. These differences remain a controversial issue.

THE PRESSURE SCALE OF SHOCKS

The reader is invited to consult excellent published introductory articles and books on the physics of shocks (Langenhorst & Hornemann 2005, Melosh 1989, Sharp & DeCarli 2006). Impacts produce shocks when the velocity of deformation exceeds the velocity of sound in matter. The shock wave propagates and compresses the materials, generating irreversible effects such as heating and plastic deformation. **Figure 3*a*** describes a simple situation in which one can define the different shock parameters. The impact of the projectile onto the target (time t_0) creates a shock wave, setting up a shock front that travels at velocity U_s into both target ($U_s = U_t$) and projectile ($U_s = U_p$). The impacted surface starts to move with a velocity u, called the particle velocity, in the projectile ($u = u_p$) and the target ($u = u_t$). At a later time t, the shock wave has propagated in the target through a distance $U_t(t - t_0)$ and the impacted surface through a less important distance $u_p(t - t_0)$. Once the shock compression event ends, rarefaction waves from surrounding regions of low pressure propagate into the compressed region and lower its pressure to ambient conditions.

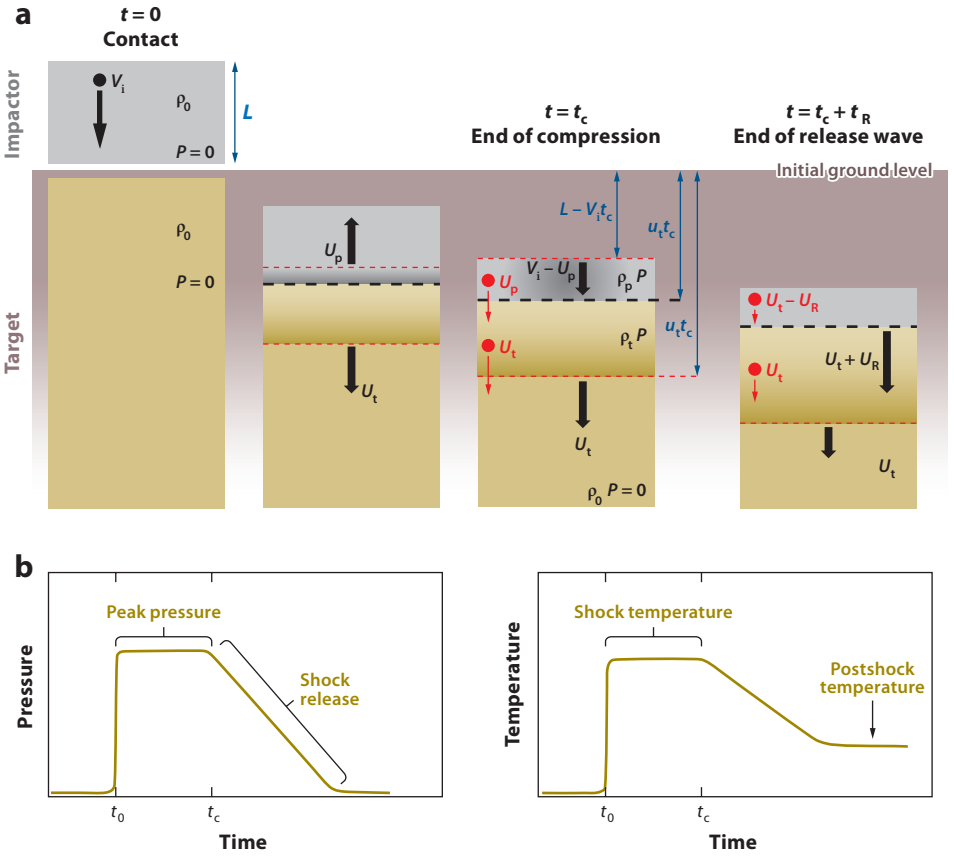

Figure 3

(*a*) Propagation of shock waves in the impactor/target system. Subscript t refers to the target and subscript p to the impactor (projectile). U_t and U_p are the respective shock front velocities in the target and projectile; u_t and u_p are the respective particle velocities. The density is ρ, and the pressure is *P*. Adapted from Melosh (1989). (*b*) Qualitative variations of pressure and temperature during a shock event. The plateau during which pressure is constant is usually referred to as the continuum pressure state of the shock. The time duration of this plateau can be estimated with Equation (1). Complete cooling to ambient conditions takes a longer time.

This decompression is generally adiabatic and, to a good approximation, isentropic. **Figure 3*b*** shows the qualitative way pressure and temperature vary during a shock event.

U_s and *u* are related, through the Rankine-Hugoniot equations, to the pressure (*P*), density (ρ), and internal energy (*E*) before and after the passage of the shock front (Langenhorst & Hornemann 2005). From these equations, the following relationships can be derived between the particle and shock velocities, density, and pressure:

$$P - P_0 = \rho_0 U_s u. \tag{3}$$

In addition to the Hugoniot formalism of shocks, numerous laboratory experiments have shown that, for a given material, there exists a linear relationship between U_s and *u* (Sharp & DeCarli 2006):

$$U_s = C_0 + Su, \tag{4}$$

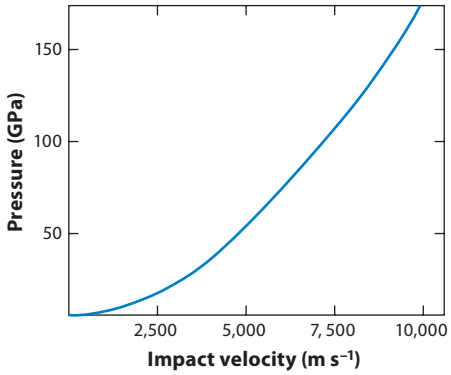

Figure 4

Relationship between impact velocity and continuum shock pressure for a basaltic impactor/target system.

where C_0 and S are constants proper to the material. C_0 corresponds to the ambient pressure sound velocity, and S is directly related to the Grüneisen parameter. Equation (3) can thus be rewritten:

$$P - P_0 = \rho_0 u(C_0 + Su). \tag{5}$$

The curve represented by this equation is known as the Hugoniot. The Hugoniot curves are graphical representations of all the final states that can be attained in a material by a given shock wave. Our purpose is to use Equation (5) to put constraints on the pressures that can be reached during natural shocks with typical impact velocities (v_i) up to 30 km s^{-1}. Finally, the impact and particle velocities are related through (Melosh 1989)

$$u = \frac{v_i}{2}. \tag{6}$$

Equation (5) can thus be rewritten:

$$P - P_0 = \rho_0 \frac{v_i}{2}\left(C_0 + S\frac{v_i}{2}\right). \tag{7}$$

Figure 4 illustrates the relationship between the impact velocity and the pressure generated during a shock between two basaltic bodies (basalt is a typical planetary material). For an impact velocity of 5 km s^{-1}, the pressure generated is approximately 50 GPa. Pressures in excess of 100 GPa (the static pressure at 2,300 km inside Earth) are reached for impact velocities greater than 7.5 km s^{-1}. Notice that the maximum pressure attained during a shock relies only on the impact velocity and material properties.

THE TEMPERATURE SCALE OF SHOCKS

During a shock, an important part of the irreversible deformation of the material is converted into heat. This adiabatic increase of the material temperature at the highest pressure can be estimated by integrating the following equation (Benzerara et al. 2002, Langenhorst & Hornemann 2005):

$$dT = \frac{V_0 - V}{2C_V} dP + \left(\frac{P - P_0}{2C_V} - T\frac{\gamma}{V}\right) dV, \tag{8}$$

in which P is the pressure and V the specific volume (the index 0 denotes an initial value); T is the temperature along the Hugoniot; γ is the Grüneisen parameter (taken as a constant value); and C_V is the molar heat capacity at constant volume. This equation is derived from the Rankine-Hugoniot

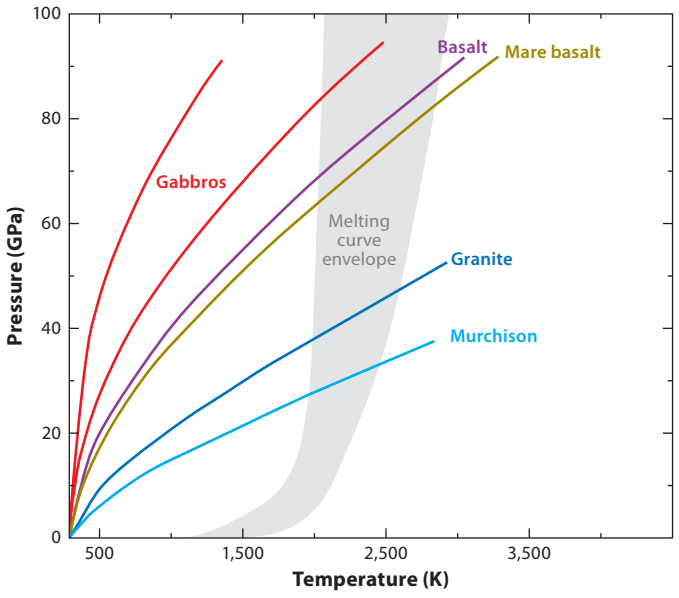

Figure 5

Relation between continuum shock pressure and shock temperature for different rocks. The Hugoniot curves for different rocks are shown. Murchison is a chondrite meteorite. The shock temperatures can reach thousands of Kelvins for shocks above 100 GPa. The melting curve envelope contains most of the known or extrapolated data for granites, basalts, peridotites, and meteorites [see, for instance, Fiquet et al. (2010)]. Granites melt at a much lower continuum shock pressure than gabbros. The difference between basalts and gabbros is due to porosity and mineralogical differences (glass versus crystals).

equation combined with the classical thermodynamic relation that relates internal energy variations to changes in entropy and volume. The postshock temperature is obtained by adiabatic decompression to 1 bar using

$$\frac{T_0}{T_1} = \left(\frac{V_1}{V_0}\right)^{\gamma}. \quad (9)$$

Figure 5 shows the calculated peak temperature as a function of pressure for different rocks, assuming an initial temperature of 300 K. (P,T) curves such as the one presented in **Figure 5** can be used to predict mineral transformations and rock melting for typical shock conditions and materials. Granites and chondrite meteorites melt at much lower shock pressures than do basalts, gabbros, and peridotites.

To determine shock temperatures for real polymineralic rocks, one must also account for the effects of porosity, grain boundaries, and compositional heterogeneity on deformation. Typical rock porosity ranges from a few percent for compact rocks such as basalts to 25% for sandstones. Moreover, compressional shock waves do not propagate at the same speed in different minerals. In a natural shock event, all these structural heterogeneities will produce shock pressure spikes at the shock front that can vary in magnitude from grain to grain. Similarly, large transient local temperature differences can be produced. Assuming a mineral grain size of approximately a millimeter, pressure heterogeneities will equilibrate in less than a fraction of microsecond (for a typical shock velocity of 10 km s^{-1}), whereas temperature heterogeneities require fractions of seconds to equilibrate (for the typical thermal diffusivity in minerals, 10^{-6} m^2 s^{-1}).

A major effect of porosity during a shock is that the compaction and closure of pore space enhance the heat generated by shock wave compression. A porous material thus melts at lower peak shock pressures than a nonporous material. Additionally, the compaction of pores consumes a significant amount of the shock energy and leads to a pronounced shock wave decay. As described below, shocked rocks encounter local melting conditions at a millimeter scale in the form of shock melt pockets (MPs) (Wunnemann et al. 2008).

NUMERICAL MODELING OF IMPACTS

Prior to recent advances in numerical modeling capacity, it was difficult to understand the spatial distribution and degree of metamorphic transformation in an impact crater. This limitation was due primarily to the complex history of block ejections (the mixing of melt and solid blocks from different parts of the crater). Models now provide the necessary guidelines to understand the dynamic and geometrical aspects of impact metamorphism (Collins et al. 2012; Ivanov 2005; Jutzi et al. 2008, 2009). They permit the exploration of the pressure, temperature, and time (P,T,t) history undergone by rocks, as well as the prediction of the amount of deformation and the distance over which ejecta are displaced from their initial location. An example of such a simulation is shown in **Figure 6**. The isobars (corresponding to the peak pressures) and the isotherms (related to the compression's work transformed into heat) are more or less spherically oriented with respect to the center of the impact. The maximum pressure and temperature conditions decrease radially and will last the time of the compression phase.

The spatial variation of the (P,T) conditions poses questions. For a given impact, ejected rocks can come from regions very near the crater center (highest continuum pressure) but also from regions relatively far from the center (lowest continuum pressure). If the initial sample location is poorly documented, it becomes impossible to estimate the highest pressure generated during the shock. The problem is even worse for meteorites, for which the crater on the parent body is unknown. Estimating the impact velocity from the pressure-induced transformations of rocks and minerals is thus a difficult exercise. Notice that the continuum shock pressure duration is the same for all the samples.

THE MINERALOGICAL RECORD OF SHOCKS IN ROCKS: WHAT DO WE EXPECT? WHAT DO MODELS PREDICT?

Owing to pressure and temperature variations, rocks subjected to a shock will undergo transformations that are mechanical (i.e., brecciation, fracturing), chemical, and mineralogical (i.e., amorphization, melting, vaporization, high-pressure phase transformations). These transformations take place at much higher rates than in usual metamorphism. We do not review all these changes in detail but rather take a few examples to emphasize the major processes and the remaining unsolved issues. The reader is invited to consult the numerous existing review papers (El Goresy et al. 2013; Gillet et al. 2007; Langenhorst & Deutsch 2012; Sharp & DeCarli 2006; Stöffler et al. 1988, 1991).

Numerical simulations of impact are fundamental for understanding the mineralogical record in shocked rocks. Let us use the SiO_2 chemical system (**Figure 7**) in conjunction with the result of a simulation (Wunnemann et al. 2008). The SiO_2 phase diagram is complex, especially because of the solid phases that are stable at different pressure and temperature conditions. It is well suited for looking at impact sites in which SiO_2-rich rocks are dominant.

After they were synthesized in the laboratory (Coes 1953, Stishov 1963), coesite and stishovite were the first high-pressure polymorphs of minerals found in impact rocks (Chao et al. 1962,

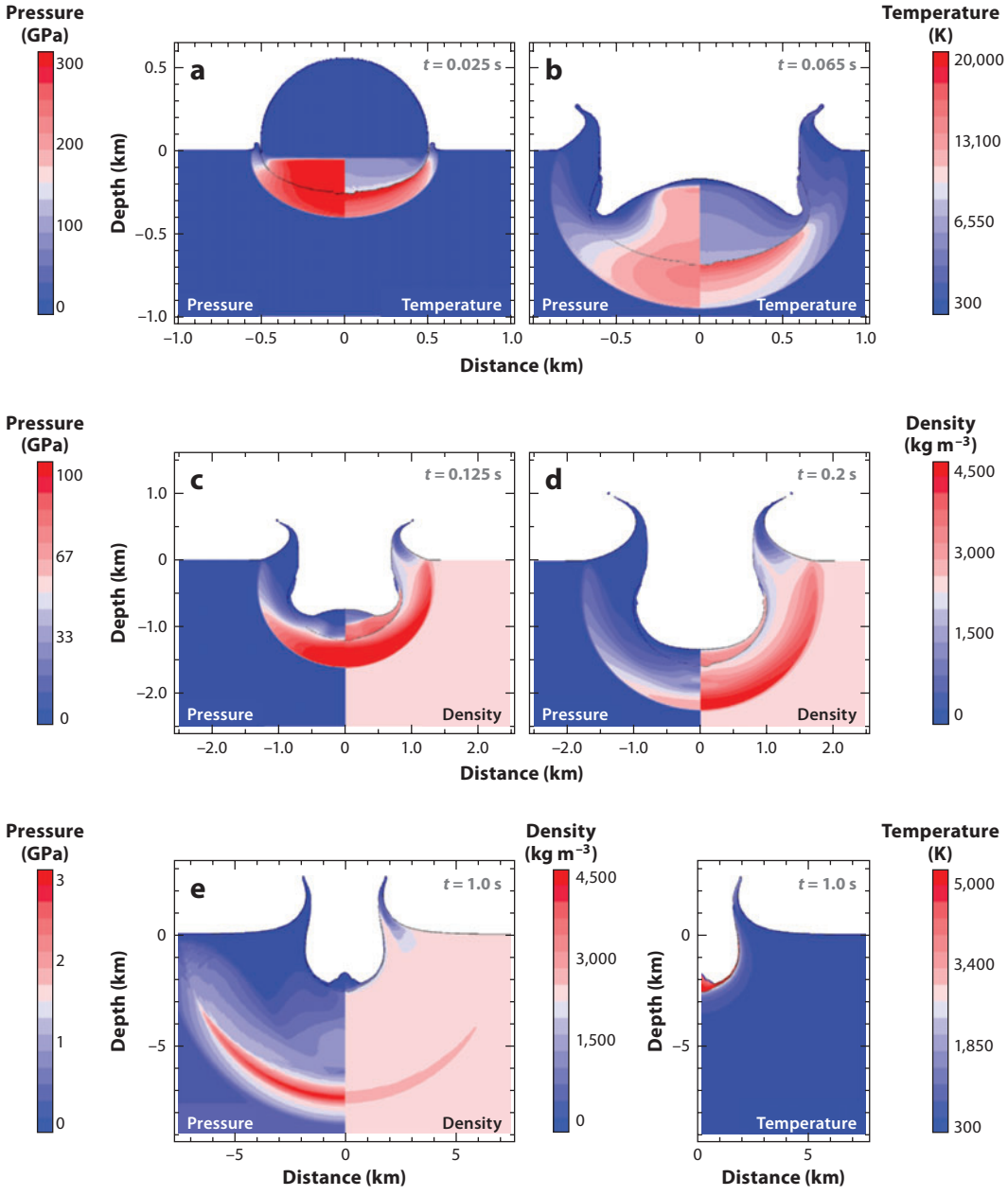

Figure 6

Results of a numerical simulation that show, with greater detail than in **Figure 3**, the propagation of the shock waves in both the impactor and target. Cross sections are shown at different times (t) after the contact (Collins et al. 2012, Wunnemann et al. 2008) when a 1-km-diameter dunite impactor hits a granite target at 18 km s^{-1}. (*a*) A region of high pressure develops along the interface just at the beginning of the contact. Both target and impactor are compressed and deform. The rear of the impactor is unaffected by events that occur at the contact region. (*b*, *c*) The shock wave in the impactor reaches its rear surface and is reflected as a release wave that is responsible for impactor decompression to lower pressures. (*d*) The shock wave in the target propagates spherically and is followed by the release wave. (*e*) Behind the shock wave, the plume of vapor and ejecta begins to expand, and the excavation phase starts. Courtesy of G.S. Collins.

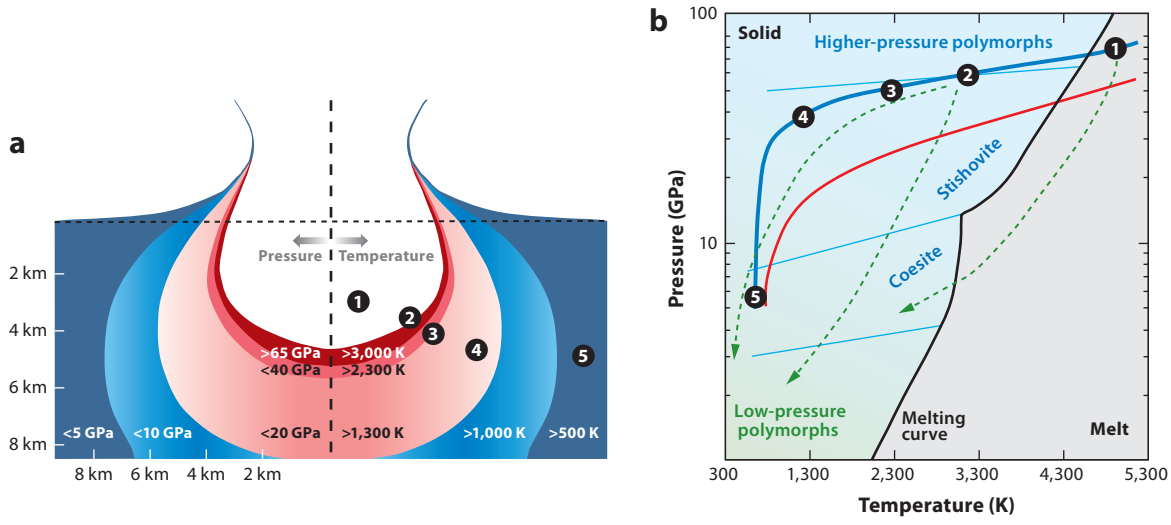

Figure 7

(*a*) Peak shock pressure and temperature distribution in a quartzite target at the end of the compression phase. The impact velocity was 12 km s^{-1} and the projectile diameter was 2 km. For such conditions, the compression phase lasts 1/6 s. The isobars and isotherms are more or less spherically disposed with respect to the center of the impact. These maximum pressure and temperature conditions decrease radially. The ejected material comes from zones that underwent different (*P*,*T*) conditions. Modified from Wunnemann et al. (2008). (*b*) Phase diagram of silica, showing the Hugoniot curves of nonporous (*blue*) and porous (*red*) sandstone. The solid black curve corresponds to the melting curve of SiO_2. The light blue lines correspond to the polymorphs' transition curves. The low-pressure SiO_2 phases are quartz, tridymite, and cristobalite. The higher-pressure polymorphs are seifertite (α-PbO_2 structure) and a $CaCl_2$-type structure. Numbers on the quartzite Hugoniot correspond to those in panel *a*. Dashed green curves correspond to hypothetical decompression (*P*,*T*) paths. Modified from Langenhorst & Deutsch (2012).

Kieffer et al. 1976). They have so far been described in more than ten impact sites, including the Ries crater, the Barringer crater, and the Vredefort impact structure (French & Koeberl 2010, Stahle et al. 2008). Other phases of silica are often found on such sites, including low-pressure crystalline phases such as cristobalite and tridymite as well as various amorphous phases that result from solid-state amorphization of crystals (diaplectic glass) or quenching of a former melt at high or low pressure. Finally, specific deformation features called planar dense features (PDFs) are often observed in shocked quartz crystals. These PDFs appear in laboratory shock experiments between 10 and 35 GPa. They are also often encountered in shocked feldspars. These damaged minerals, together with the quenched high-pressure minerals, are often used as shock indicators. However, their use in understanding impact processes requires knowledge of their exact nature: how, when, and where they can form.

In **Figure 7**, we have positioned the pressure (*P*) and temperature (*T*) stability fields of some of the SiO_2 phases together with a simulation of an impact on quartzite. The Hugoniot curves of nonporous and porous material are shown (Wunnemann et al. 2008), indicating the final *P* and *T* conditions reached by rocks located at different distances from the impact point as well as those attained by the ejected blocks. Some indicative decompression paths are also shown. The presence of one or the other form of SiO_2 in a rock sampled in the field will depend on three main parameters: (*a*) the peak pressure (which, due to the radial decrease of pressure, depends on the original location in the crater); (*b*) the decompression path and the kinetics of the different phase changes; and (*c*) its Al_2O_3 content (Lakshtanov et al. 2007). For instance, point 2 in **Figure 7** is in the stability field of stishovite; this polymorph can form if the time the shocked rocks remain in its stability field is long

enough and in agreement with its nucleation and growth rates, which are commensurate with its grain size (Kubo et al. 2010). Moreover, this high-pressure polymorph will be preserved only if the decompression path leads to efficient cooling, preventing the back-transformation of stishovite into a low-pressure polymorph or a melt. Coesite and stishovite can also crystallize from a melt formed at high pressure, because the whole rock has been sufficiently heated and the release paths have passed through the stability fields of the high-pressure polymorphs (see point 1 in **Figure 7**). This qualitative example shows the complexity of recovering the impact characteristics from the (P,T,t) history recorded in rocks and minerals.

WHY, HOW, AND WHERE DO HIGH-PRESSURE MINERALS FORM IN SHOCKED ROCKS?

We now discuss how minerals and their transformations can record part of the history of a shock. We focus on the role of preexisting defects within the rocks, which can lead to a significant localized temperature increase during the passage of the shock wave, creating localized zones where the (P,T,t) history of a rock sample is better recorded.

Shock pressure is a crucial parameter because it is directly related to the relative impact velocity between the target and the projectile (**Figure 4**). Until very recently, pressure was estimated by a relative scale based on the presence of vitrified minerals and their refractive indices, the density of PDFs and other deformation features, and the presence of shear melt veins (SMVs) or MPs (Stöffler et al. 1988, 1991; Stöffler & Langenhorst 1994). This scale was calibrated through laboratory dynamic recovery experiments in which the shock duration is on the order of a microsecond, far too short to permit the nucleation of high-pressure minerals; however, it is no longer considered valid in many cases because it leads to much higher pressures than expected (El Goresy et al. 2013).

In the past decade, the occurrences of several high-pressure minerals formed in or near SMVs and MPs shed new light on the (P,T,t) history of shocked rocks (Gillet et al. 2007). Pressure, temperature, and time are the crucial parameters that control the stability of minerals. Let us consider a simple example: a monomineralic rock made of crystals of Mg_2SiO_4-olivine with zero porosity and perfect grain boundaries. All the shock states that this rock can attain are described by the Hugoniot curve drawn in a (P,T) diagram (**Figure 8**).

Also shown in this diagram are the stability fields of the different forms of Mg_2SiO_4—olivine at low pressure, wadsleyite, ringwoodite, and the assemblage $MgSiO_3$-perovskite + MgO-periclase at high pressure—as well as the isochrones that give the time required to transform a 10-μm-sized crystal of olivine to ringwoodite. A rock sample shocked to a state A (**Figure 8**) will not undergo a phase transition, because the (P,T) conditions remain in the stability field of olivine. For the shock state B, the transformation of olivine to ringwoodite is not achieved even if the rock is shocked in the stability field of this high-pressure phase. The temperature is not high enough to promote the diffusion of elements. To reach temperatures sufficient to induce the formation of high-pressure minerals during the typical natural shock durations (a few milliseconds to a few seconds), pressure on the Hugoniot must be close to 100 GPa (shock state C in **Figure 8**).

From the phase diagram and the Hugoniot curve, it appears that the formation of a significant proportion of high-pressure minerals in the bulk of rocks can be achieved only at very high pressure. Such massive phase changes, like the massive formation of perovskite, have never been observed in dynamic experiments or in monomineralic or polymineralic rocks in nature. However, the formation of various high-pressure minerals has been documented within, or in the close vicinity of, specific shock features encountered in shocked terrestrial rocks and meteorites: the SMVs and MPs (**Figure 9**). This formation corresponds, for instance, to a case in which, for bulk shock

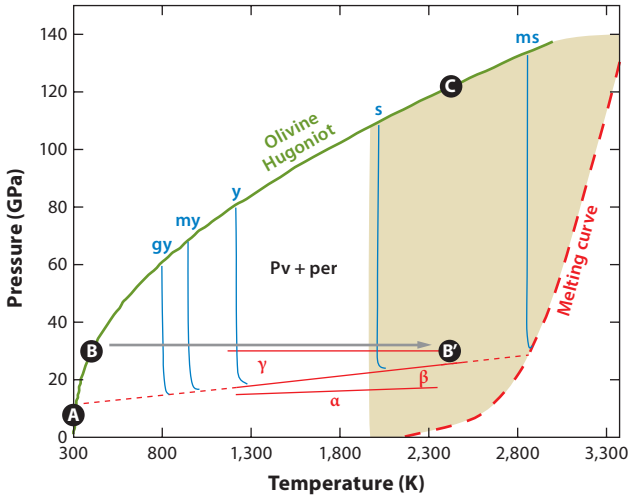

Figure 8

Phase diagram of the Mg_2SiO_4 polymorphs. The olivine Hugoniot curve is in green (Mosenfelder et al. 2007). The isochrones (gy = 109 years, my = 106 years, y = year, s = second, ms = millisecond) are calculated from experimental data and fit to a classical rate equation for interface-controlled crystal growth (Kerschhofer et al. 2000, Mosenfelder et al. 2001, Ohtani et al. 2004). See the text for a discussion of points A, B, B′, and C. Abbreviations: α, Mg_2SiO_4-olivine; β, Mg_2SiO_4-wadsleyite; γ, Mg_2SiO_4-ringwoodite; Pv, $MgSiO_3$-perovskite; per, MgO-periclase.

conditions of point B in **Figure 8**, some localized zones undergo the (*P*,*T*) conditions of point B′. The pressure is the same, but the local temperature is far higher than the bulk temperature.

SMVs and MPs are ubiquitous in shocked rocks and are related to frictional heating and porosity collapse induced by the passage of the shock waves. Local temperature differences play an essential role in the recording of pressure during a shock. For the lunar meteorite shown in **Figure 9*b***, the magmatic texture acquired after eruption on the Moon, indicative of rapid cooling, is well preserved on both the outer walls of the SMV that crosscuts the sample. No changes are observed that could indicate the passage of a shock wave. Within the vein, which exhibits typical flow texture (**Figure 9*d***), blocks of minerals have been entrained and transformed into high-pressure minerals. Pressure is the same within and outside the SMV, but the local temperature increase, greater than that induced by the whole-rock adiabatic heating, is high enough to melt the rock and form a melt vein in which the pressure is hydrostatic due to the liquid nature of the melt. With long enough peak shock pressure and sufficiently high temperature, the mineral fragments entrained in the melt vein can transform into phases that are stable at high pressure, constraining the continuum pressure of the shock. The rock fragments of different sizes in the vein were originally cold entrained. Consequently, every rock or mineral fragment in the vein had its own temperature gradient: hottest at the edges in contact with the melt in the vein and coldest at the interior. Temperature gradients between the rim and the center are larger in big fragments. The bulk of the rock retains the metastable low-pressure phases because of its relatively low temperature. The MP (**Figure 9*e***) shows the crystallization from a melt of minerals that are stable only at high pressure. We now describe how such local temperature increases can happen.

In a polymineralic rock, interfaces between minerals with different shock impedances (i.e., sound velocities), grain boundaries, and initial porosity or cracks produce wave reverberation and attenuation that strongly affect the propagation of the shock wave. Thus, the pressure

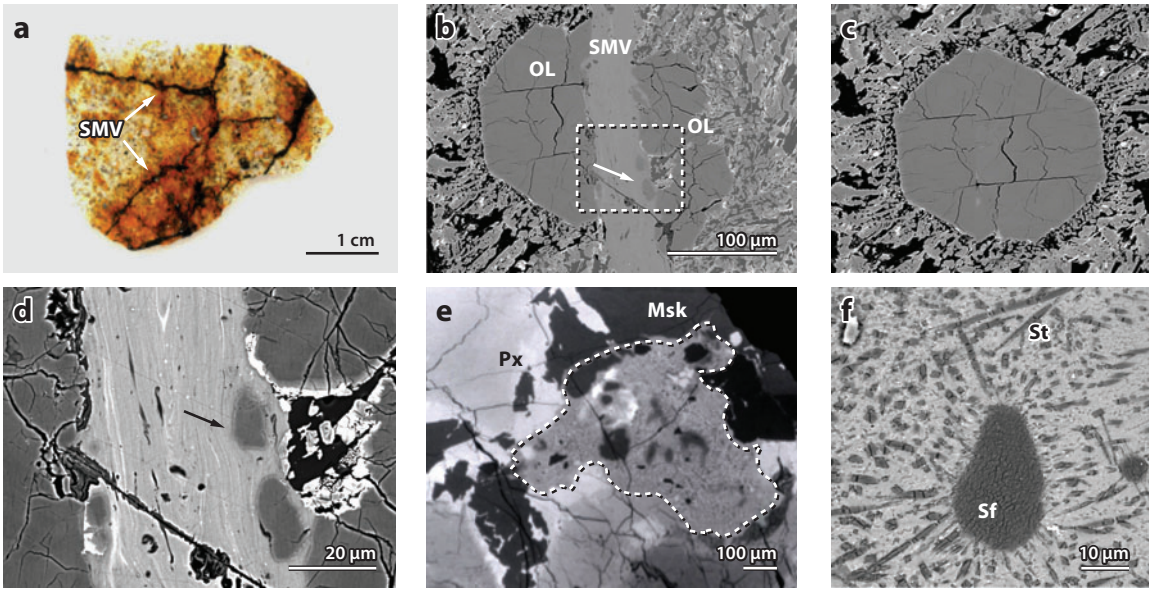

Figure 9

Typical microscopic shock features in meteorites. (*a*) Optical image of a thin section of a chondrite meteorite that contains numerous shear melt veins. The black color of the veins is due to the presence of large amounts of glass, which results from melt quench. (*b*) Thin section of a lunar meteorite (NWA 479) observed by scanning electron microscopy, showing an SMV crosscutting a single crystal of olivine. On both sides of the SMV, the pristine magmatic texture that results from lunar volcanic activity is well preserved and is neither chemically nor structurally altered by the passage of the shock wave. Fragments of olivine (*white arrow*) are entrained in the vein. (*c*) Possible texture of panel *b* before the shock (image reconstitution). (*d*) Detailed view of the dashed rectangle in panel *b*. The material within the SMV consists of glass and tiny crystals typical of a quenched melt. The olivine fragments (*black arrow*) entrained in the vein are transformed at their rims into ringwoodite, a high-pressure polymorph of olivine. Note the flow features (meanders, folds, and schlieren) indicating a low melt viscosity. (*e*) Melt pocket in the NW480 Martian meteorite (Barrat et al. 2002). The delineated zone (*dotted contour*) contains glass and high-pressure crystals of former SiO_2-seifertite or SiO_2-stishovite (*f*), indicative of the rapid quenching of the melt at high pressures. Abbreviations: Msk, maskelynite; OL, olivine; Px, pyroxene; Sf, SiO_2-seifertite; SMV, shear melt vein; St, SiO_2-stishovite.

and temperature distribution in a shocked rock is heterogeneous, and the shock features are heterogeneously distributed in both space and time.

Several simple situations are shown in **Figure 10**. The shock front and particle velocities differ from one mineral to another and can thus lead to shear stresses at the mineral interfaces (**Figure 10*a***). These shear stresses, combined to a very high shearing velocity, can nucleate SMVs, leading to local temperature increases that can be numerically modeled or estimated through simple calculations. From the equation of frictional heating (Melosh 2005), the temperature increase ΔT is

$$\Delta T = \tau \dot{\delta} \sqrt{\frac{\Delta t}{\rho K C_P}}, \tag{10}$$

which can also be written as

$$\delta_m = \frac{\kappa}{\dot{\delta}} \left(\frac{\rho C_P (T_S - T_0)}{\tau} \right)^2. \tag{11}$$

One can compute either the temperature increase for a given shear stress and displacement rate or the minimal displacement that leads through frictional sliding to a given temperature

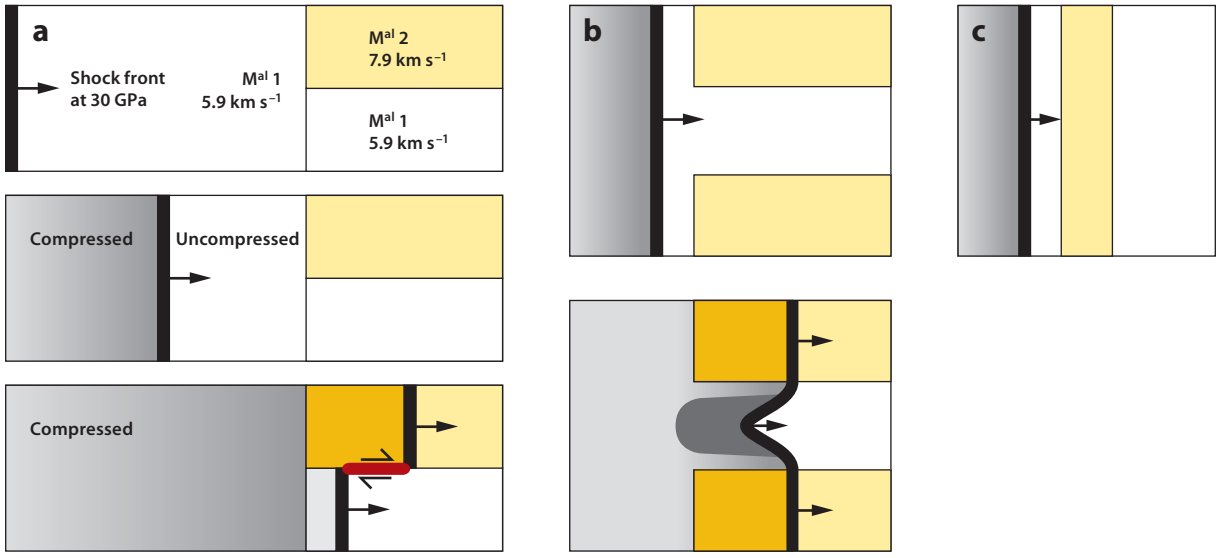

Figure 10

(*a*) A shock wave corresponding to a pressure of 30 GPa propagates through a feldspar mineral. It encounters an interface beyond which the shock front has to propagate at two different velocities, creating important shear stresses that could account for the formation of shear melt veins. (*b*) Propagation geometry in which a thin plate of feldspar is sandwiched between two olivine grains. Because of the velocity difference, the shock front is refracted, creating a zone of higher pressures in the central part of the feldspar (*dark gray zone*) because the front has to travel at the velocity for olivine. This high-pressure central region will return in a short time to 30 GPa. Temperature will also locally increase in this zone to reach the order of 2,500 K, sufficient to induce local melting (Sharp & DeCarli 2006). (*c*) See text for comments. Adapted from Biren & Spray (2011) and Sharp & DeCarli (2006).

increase. τ is the shear stress (on the order of 10^8 Pa); ρ the material density (on the order of 2,800 kg m^{-3}); C_P the specific heat at constant pressure (on the order of 1,000 J kg^{-1}); K the thermal conductivity (on the order of 2.5 W m^{-1} K^{-1}); κ the thermal diffusivity (on the order of 10^{-6} m^2 s^{-1}); $\dot{\delta}$ the displacement rate; and δ_m the displacement. For instance, using Equation (10), the melting temperature of olivine at 30 GPa, T = 2,500 K, is attained in 0.1 ms for a displacement rate of 1 m s^{-1}. These conservative values show that the initiation of melting by shearing is a very efficient process.

The formation mechanism of SMVs is likely size dependent. SMVs can range in width from a few micrometers to centimeters and even meters in the case of large pseudotachylites (Melosh 2005, Spray 2010). Small SMVs are relatively well understood. The order of magnitude of the width of the molten zone can be estimated by the length, w, over which the generated thermal anomaly is spread:

$$w = \sqrt{\kappa t}. \tag{12}$$

With typical values of t and κ one gets $w = 100$ μm. However, the formation of a molten layer lubricates the sliding zone and leads to reduced friction, which seems inconsistent with large SMVs. Melosh (2005) has proposed that melt can be extruded from the plane of sliding into adjacent fissures and sliding zones through a hydraulic fracturing mechanism. This vein feeding mechanism can account for the formation of thick veins. It can also prevent a rapid cooling of the veins and thus permit a longer record of the duration of the continuum pressure stage and of the pressure changes during the decompression.

The presence of different minerals can also lead to local pressure excursions with respect to the pressure of the whole-rock Hugoniot (Sharp & DeCarli 2006). The latter represents an average value of the shock velocity of individual minerals. However, at the scale of the mineral sizes, the shock front has an irregular shape due to shock velocity differences among minerals. A simple case is outlined in **Figure 10*b***. The shock front is refracted, due to a difference in wave velocities, and produces localized high pressures in the central part of the mineral, which has the lowest acoustic velocity. The typical size of the high-pressure zone is a few micrometers, and the pressure spike lasts only for tens of nanoseconds. A last case is shown in **Figure 10*c***. The 30 GPa front in the high-impedance mineral passes through a layer of low-impedance mineral before traveling again in a high-impedance mineral. The initial pressure attained when the shock wave enters the low-impedance mineral is less than 30 GPa because of a lower velocity. The pressure will equilibrate to 30 GPa through a sequence of successive reflections on the grain boundaries. The typical timescale for reaching pressure equilibrium, 1 μs, is obtained by dividing the typical grain size ($\approx 10^{-3}$ m) by the typical shock wave velocity ($\approx 10^{3}$ m s^{-1}). These localized pressure spikes can also lead to localized temperature increase. The temperature heterogeneities will vanish with a typical timescale of a few tens to hundreds of milliseconds, at variance with the much more abrupt pressure decrease.

Pores, cracks, and voids can also lead to important localized temperature increases during the passage of a shock wave. Porosity significantly increases the amount of heat transmitted by the shock wave to the target material by closure of the empty volume. This is first observed macroscopically when comparing porous and nonporous materials shocked under similar conditions. The porous material heats more efficiently and melts at much lower shock pressures (see, for instance, the case of SiO_2 in **Figure 7*b***). The MPs are among the clearest microscopic features of the local temperature increases. Numerous studies have ascribed their formation to a local partitioning of energy near the void pores (Beck et al. 2007, Heider & Kenkmann 2003, Mader 1965). Starting from the assumption that the initial shock energy is partitioned into temperature increase and melting enthalpy, one can write

$$\frac{P(V_0 - V)}{2} = F\,(C_\mathrm{P}\Delta T + H_\mathrm{m})\,, \tag{13}$$

where P is the continuum shock pressure, V the specific volume of the compacted material, V_0 the specific volume of the porous material, H_m the enthalpy of melting, F the fraction of molten material, ΔT the temperature increase, and C_P the specific heat. Introducing porosity ψ in the equation

$$\psi = 1 - \frac{V}{V_0} \leftrightarrow V_0 = \frac{V}{1-\psi} \tag{14}$$

and assuming $F = 1$ because the MPs are almost molten, one obtains

$$P = 2\frac{(2-\psi)}{\psi}\frac{(C_\mathrm{P}\Delta T + H_\mathrm{m})}{V}. \tag{15}$$

Using typical values ($H_\mathrm{m} = 350$ kJ kg^{-1}; $C_\mathrm{P} = 1{,}000$ J kg^{-1}; $V = 3.3 \times 10^{-4}$ m^3), one finds that a temperature of 2,500 K can be reached for a shock pressure of 30 GPa and a local porosity of 0.4.

HIGH-PRESSURE MINERALOGY OF SHOCKED TERRESTRIAL ROCKS AND METEORITES: EXAMPLES AND QUESTIONS

Natural high-pressure minerals in meteorites have been studied extensively for 40 years (Binns 1970). Natural shock conditions have produced many of the phases that form at high pressure in

Table 2 Major high-pressure minerals observed in shocked terrestrial rocks and meteorites

Mineral name[a]	Structure	Simplified formula	Rock type	Reference(s)
Wadsleyite	Modified spinel	$(Mg,Fe)_2SiO_4$	Meteorite	Price et al. (1979)
Ringwoodite	Spinel	$(Mg,Fe)_2SiO_4$	Meteorite	Binns (1970), Chen et al. (1996), Xie & Sharp (2003)
Majorite	Garnet	$(Mg,Fe,Ca,Na,Al)SiO_3$	Meteorite, Earth	Chen et al. (1996), Stahle et al. (2011), Xie & Sharp (2003)
Akimotoite	Ilmenite	$(Mg,Fe,Ca)SiO_3$	Meteorite	Ferroir et al. (2008), Sharp et al. (1997), Tomioka & Fujino (1997)
	Perovskite	$(Mg,Fe,Ca)SiO_3$	Meteorite	Miyahara et al. (2011), Sharp et al. (1997), Tomioka & Fujino (1997)
Lingunite	Hollandite	$(Na,Ca,K)AlSi_3O_8$	Meteorite, Earth	Gillet et al. (2000), Langenhorst & Dressler (2003), Langenhorst & Poirier (2000a)
	Hexaluminosilicate	$(Ca_x,Na_{1-x})Al_{3+x}Si_3O_{11}$	Meteorite	Beck et al. (2004)
Magnesiowüstite	NaCl	$(Mg,Fe)O$	Meteorite	Chen et al. (1996), Xie & Sharp (2003)
	Titanite	$(Mg,Fe,Ca)Si_2O_5$	Meteorite	Langenhorst & Poirier (2000b)
Coesite	Coesite	SiO_2	Meteorite, Earth	Ohtani et al. (2011), Stahle et al. (2008)
Stishovite	Rutile	SiO_2	Meteorite, Earth	Beck et al. (2004)
Seifertite	α-PbO_2	SiO_2	Meteorite	Sharp et al. (1999)
	Baddeleyite	TiO_2	Earth	El Goresy et al. (2001a)
Akaogite	α-PbO_2	TiO_2	Earth	El Goresy et al. (2001b)
Diamond, lonsdaleite	Cubic and hexagonal diamond	C	Meteorite, Earth	El Goresy et al. (2001c), Nakamuta & Aoki (2000)
	Clathrate?	C	Meteorite, Earth	El Goresy et al. (2003), Ferroir et al. (2010)
	$CaTi_2O_4$	$FeCr_2O_4$	Meteorite	Chen et al. (2003)
	γ-$Ca_3(PO_4)_2$	$Ca_3(PO_4)_2$	Meteorite	Xie et al. (2002)

[a]Shaded boxes indicate that the mineral has not been named.

the bulk mantle or subducting lithosphere at the (P,T) conditions of the upper mantle, transition zone, or lower mantle.

The transformations of $(Mg,Fe)_2SiO_4$-olivine into $(Mg,Fe)_2SiO_4$-wadsleyite and $(Mg,Fe)_2SiO_4$-ringwoodite are among the most extensively studied and were the first to be described in natural samples, namely in shocked meteorites (see Gillet et al. 2007 for a review). Rather than providing a comprehensive review of the mineralogy of shocked rocks, we focus on a few selected examples that illustrate several of the concepts previously discussed. **Table 2** gives a summary of the high-pressure minerals that have been reported so far in terrestrial and extraterrestrial shocked rocks.

The Formation of the High-Pressure Polymorphs of $(Mg,Fe)_2SiO_4$ and $(Mg,Fe)SiO_3$ and the Timescale of Shocks in Meteorites

The results from experimental petrology (phase diagrams and kinetics) can be applied to shocked rocks to decipher the time durations of the impact and the continuum pressure of the shock. We

have seen that the duration of the peak pressure experienced by meteorites or terrestrial rocks can vary over at least three orders of magnitude (**Table 1**). In shocked meteorites, glasses are found together with high-pressure minerals within MPs, indicating an efficient quenching while at high pressure or at the onset of postshock decompression. The melting textures observed in the SMVs are also similar in terms of crystal size and shape to those observed in high-pressure assemblages synthesized in high-pressure and high-temperature experiments.

Single minerals, or even polymineralic fragments, can be cold entrained into SMVs (**Figure 9**). Subjected to the transient high pressures from the passage of the shock wave, these fragments undergo metamorphic transformations. The most abundant meteorite-forming minerals—olivines, pyroxenes and feldspars—are often transformed into polymorphs or mineral assemblages only stable at high pressures (Gillet et al. 2007).

The $(Mg,Fe)_2SiO_4$ polymorphs of olivine (**Figure 8**) are well suited to show how and where high-pressure minerals can form during the passage of a shock wave and the crucial role of local temperature increases caused by rock heterogeneities. They can either form by a solid-state transformation or result from the crystallization of a melt at high pressure. These transformations can be observed in the walls of SMVs, in olivine fragments entrained in SMVs, or as a result of fractional crystallization from monomineralic olivine melts (Miyahara et al. 2008).

The SMV in **Figure 11** has been observed in the Yamato 791384 L6 chondrite (Miyahara et al. 2010). The SMV contains glass, $(Mg,Fe)SiO_3$-majorite and (Mg,Fe)O-magnesiowüstite, and remnants of $(Mg,Fe)SiO_3$–perovskite, which indicate that the melt crystallized at a pressure of 24 GPa and a temperature of at least 2,500 K. These conditions fix the continuum shock pressure. The texture, grain size, and chemical composition of the constituents of this assemblage are very similar to those of their counterparts produced in static multianvil experiments, indicating that equilibrium was reached (Kerschhofer et al. 1996).

The transformation into ringwoodite of olivine grains in contact with the SMV shows a specific arrangement and can be used to infer a minimum duration of the shock. Close to the SMV, ringwoodite is polycrystalline. At a few tens of micrometers away, it forms a set of oriented and polycrystalline zones; at 50 micrometers away, only very thin (10 nm) single lamellae showing well-defined crystallographic relationships with the host olivine are observed. This arrangement reflects the temperature dependence of the transformation kinetics (**Figure 8**). Far from the SMV, the temperature increase due to heat diffusion is too low to induce the transformation, whereas close to the SMV, the temperature increase is great enough to produce an almost complete transformation. The chemical composition of ringwoodite is similar to that of olivine. The shock pressure is efficiently recorded in or near the SMV by the formed high-pressure minerals. Far from the SMV, the shock pressure cannot be inferred; only very crude estimates can be made through deformation features, which are poorly calibrated as a proxy for pressure. The whole rock experiences (P,T) conditions on the Hugoniot curve (point B in **Figure 8**), but locally, the temperature increase associated with the SMV translates the (P,T) conditions to point B′, where the kinetics of the transformation is much more rapid. Very recently, Miyahara et al. (2011) observed in a Martian meteorite the breakdown of $(Mg,Fe)_2SiO_4$-olivine at the wall of an SMV into the assemblage $(Mg,Fe)SiO_3$-perovskite + (Mg,Fe)O-magnesiowüstite.

From the kinetics of the olivine-ringwoodite transformation and the modeled temperature history of the vein (**Figure 8**), one can estimate the duration of the shock [see, for instance, Xie et al. (2006) or Miyahara et al. (2010)]. Typical inferred shock duration for chondrites spans the range from 100 ms to a few seconds. If one takes a typical impact velocity of 5–10 km s^{-1}, the typical order of magnitude of the impactor size ranges between a few hundreds of meters and 10 km (Beck et al. 2005).

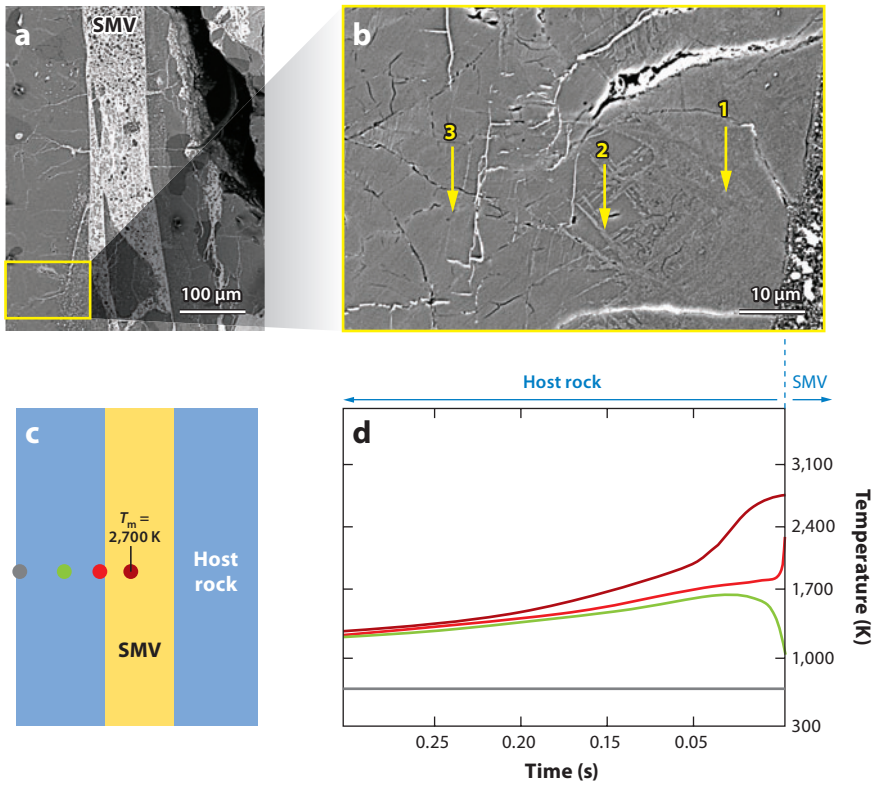

Figure 11

(*a*, *b*) Formation of ringwoodite near a shear melt vein (SMV) of a shocked L6 chondrite [after Miyahara et al. (2010)]. (*a*) General view of the SMV (scanning electron microscope image). (*b*) Detail of an olivine crystal in contact with the SMV. The incoherent transformation into ringwoodite is almost complete up to 20 μm away from the SMV (*arrow 1*) but becomes progressively less important (*arrow 2*) and by approximately 60 μm away from the SMV is not observed (*arrow 3*). Beyond 50 μm, coherent nucleation and growth of ringwoodite lamellae take place along stacking faults parallel to the (100) crystallographic plane of olivine. (*c*, *d*) Cooling model of an SMV [after Xie et al. (2006)]. The colored points in panel *c* correspond to the curves in panel *d*. These different points have contrasting cooling curves. In this model, after 30 ms, the temperature is less than 1,300 K and does not permit the further transformation of olivine into ringwoodite. T_m is the temperature of the melt.

Very often, the solid-state formation of ringwoodite and wadsleyite is observed in olivine grains entrained in SMVs. In some cases, the formation of ringwoodite can result from the fractional crystallization at high pressure of molten olivine (Miyahara et al. 2008). The fate of an olivine crystal entrained in an SMV is shown in **Figure 12**. The olivine crystal is transected by lamellae that can cross each other and can lead in some parts of the crystal to a complete transformation of olivine into wadsleyite and ringwoodite. The central parts of the lamellae are mainly composed of ringwoodite, whereas the rims on both sides are made of wadsleyite. The polymorphs also have different chemical compositions. Ringwoodite is richer in Fe than the host olivine. The Fe enrichment of ringwoodite decreases from the centers of the lamellae toward the rims. In contrast, wadsleyite is strongly depleted in Fe. Only a high-pressure melting of olivine along specific crystallographic planes followed by a high-pressure fractional crystallization of ringwoodite and wadsleyite can account for the observed crystallization textures perpendicular to the lamellae and

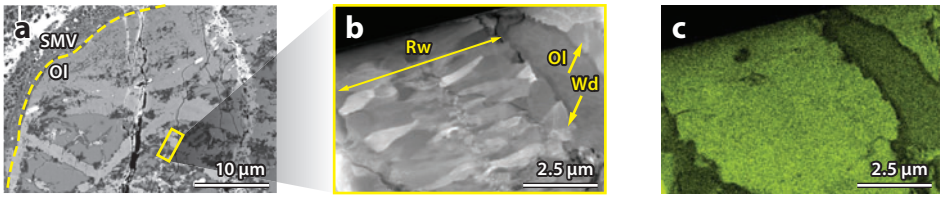

Figure 12

Formation of ringwoodite and wadsleyite by fractional crystallization (T. Ferroir, M. Miyahara, A. El Goresy & Ph. Gillet, unpublished results). (*a*) Scanning electron microscope image of a single crystal of olivine entrained in an SMV. The limit between the SMV and the crystal is outlined by the dotted yellow line. The olivine crystal is transected by numerous veins, most of which are formed of ringwoodite. (*b*) Detailed view of the yellow rectangle in panel *a*, showing a spatial arrangement that suggests crystallization of ringwoodite from an olivine magmatic liquid with elongated crystals perpendicular to the wall of the vein. A thin layer of wadsleyite at the olivine-ringwoodite interface is observed. (*c*) Chemical maps of the Fe content of the different phases. Ringwoodite is significantly richer in Fe than are wadsleyite and olivine. Fractional crystallization from a melt can explain both the spatial arrangement of the various phases and their contrasting Fe content (Miyahara et al. 2008). Abbreviations: Ol, olivine; Rw, ringwoodite; SMV, shear melt vein; Wd, wadsleyite.

for the variation in Fe content of the different phases (Miyahara et al. 2008). Shock can also induce very high structural disorder in olivine that could lead to the formation of metastable polymorphs (Van de Moortele et al. 2007a,b).

Trapping Planetary Gases: The Case of Martian Meteorites

We have explained why and how a shock wave encountering a void can lead to local temperature increase and melting. The melt may incorporate and preserve gases from these voids. The chemical signature of these gases has been important in understanding the history of meteorites such as shocked SNC meteorite EETA 79001. In this meteorite, the gas trapped in the glass and MPs was similar in composition to the Martian atmosphere as measured by the Viking Mars modules (Bogard & Johnson 1983); this has been the key argument for inferring the Martian origin of the SNC meteorites.

Entrapment of atmospheric gases is made possible by the presence of local heterogeneities within the rocks and the passage of the shock wave. On Mars, prior to the shock, the basaltic rocks that became the SNC meteorites most likely had a porosity of a few percent, typical of volcanic rocks. The voids were connected to and thus filled with Martian atmosphere. The passage of a shock front in the porous zone induces both collapse and closure of the voids and cracks connected to the atmosphere, triggers local melting, and forces solubilization of the atmospheric gases in the melts and crystals formed in the MP. After the shock front has passed, pressure drops rapidly while the temperature decrease is controlled by thermal diffusivity. To retain the Martian atmospheric signature in the MPs, efficient temperature quench is required to limit the diffusion of the gas species within the melt and quenched glass. Simple calculations (Beck et al. 2007) give a rapid quench that supports this history of the SNC meteorites.

Carbon: Diamonds and Ultrahard C Phases

Diamonds can be formed in different natural environments: at low pressure and moderate temperature around red giant stars, in the Earth at depth greater than 150 km, and in shocked terrestrial

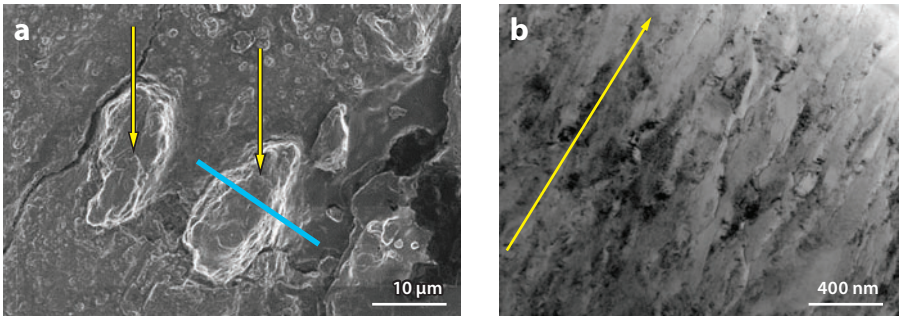

Figure 13

Shock diamonds in the Haverö ureilite (T. Ferroir, M. Miyahara, A. El Goresy & Ph. Gillet, unpublished results). Ureilites are meteorites that contain, besides olivine and pyroxene, large amounts of carbon phases, mainly graphite and diamond. Some ureilites are heavily shocked, and former graphite crystals can be transformed into diamond or other phases. (*a*) Scanning electron microscope image of a ureilite section that has been polished with diamond paste. Some parts (*yellow arrows*), nearly pure carbon, stand out by more than 10 μm in relief over the surface of the silicate matrix, suggesting that they were not easily polishable by a diamond paste and therefore have higher polishing hardness. The blue line delineates the section observed in panel *b*. (*b*) Transmission electron microscope image showing a well-defined elongated fabric of interlayered lonsdaleite-diamond-graphite (*yellow arrow*).

rocks and shocked meteorites. Diamonds were discovered in shocked rocks only as recently as 1972 by Masaitis et al. (1972) in demineralization residues from the Popigai impact site in Russia; they were later discovered in the Ries crater in Germany as well (Rost et al. 1978). A long controversy followed over whether these diamonds were formed through a chemical vapor deposition mechanism in the vapor plume generated by the impact, or by the shock wave, through a solid-state transformation of preexisting graphite or C-rich phases.

The latter scenario was confirmed by the observation of coexisting graphite and diamond crystals in thin sections in gneisses from the Ries crater (El Goresy et al. 2001c), in which diamond crystals often mimic the hexagonal shape of the former graphite. The transformation of graphite into diamond is most often observed when the initial graphite crystals are in contact with highly incompressible minerals (e.g., garnets or TiO_2-rutile). This observation emphasizes the role of shock reverberation at interfaces between compressible and less compressible minerals (see **Figure 10**) in locally increasing the temperature and thus the transformation kinetics.

New forms of C or interlayered diamond/graphite compounds with unusually high polishing hardness (**Figure 13**) have recently been discovered in shocked terrestrial rocks and meteorites (El Goresy et al. 2003, Ferroir et al. 2010). Ferroir et al. (2010) reported evidence for the natural existence of a new ultrahard rhombohedral carbon polymorph with a structure similar to diamond but with a partial occupancy of some of the carbon sites. They also reported the natural occurrence of the theoretically predicted 21R diamond polytype. These findings are of great interest for better understanding the world of carbon polymorphs and diamond polytypes because they offer new natural materials for investigating modes of formation. The discovery of these new C forms opens new avenues for research in the carbon system using either an experimental (Mao et al. 2003) or a theoretical (Blase et al. 2004, Li et al. 2009) approach.

Glass: Pressure-Induced Amorphization and Quenched Melts

Amorphous solids, or glasses, are produced in nature by either supercooling of liquids or pressurization of crystals. A liquid (melt) solidifies to a thermal glass when it is cooled—i.e., quenched—to

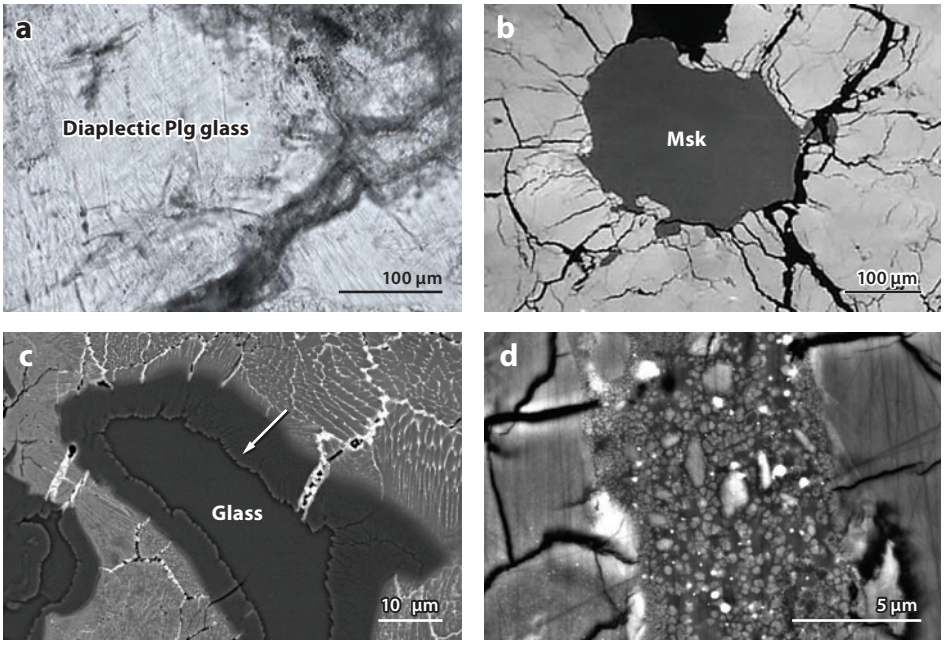

Figure 14

Different types of glasses encountered in shocked rocks. (*a*) Shocked plagioclase feldspar in a shocked granite from the suevite of the Ries crater (Germany). Different sets of crystallographically oriented, shock-induced PDFs are visible; they correspond to a thin region of diaplectic glass and are amorphous. (*b*) Maskelynite in a Martian meteorite. Until recently, this phase was interpreted as a diaplectic glass resulting from the amorphization of plagioclase. The absence of inside fractures and the presence of radial fractures in the surrounding minerals have been interpreted as results of the quenching of a melt at high pressures. (*c*) Residual glass in a Martian meteorite. The temperature drop has stopped the crystallization of a feldspar melt formed at high pressure (the white arrow indicates the crystallization front) and has left a residual melt that has been quenched to a glass. (*d*) Intimate mix of nanometric high-pressure crystallites within a glassy matrix (lunar meteorite NWA 479). Abbreviations: Msk, maskelynite; Plg, plagioclase.

below the melting point faster than it can diffuse, preventing crystallization. This quenching can occur either at high or low pressure. There is another, less common way to form an amorphous solid. Pressure-induced amorphization has been observed experimentally and naturally in many different crystalline materials, during either dynamic or static experiments. Initially discovered in ice (Mishima et al. 1984), pressure-induced amorphization is a low-temperature process that leads to the formation of dense glasses through the cold static compression of crystalline solids (Richet & Gillet 1997). It is the only way for a crystal to adapt its volume to high compression at temperatures at which diffusion is too slow to permit the crystallization of high-pressure minerals. The shock-induced glasses are called diaplectic glasses.

In shocked rocks, thermal glasses are usually free of defects and do not exhibit fractures and PDFs. Thermal glasses quenched at high pressures and those quenched at low pressures can be differentiated using simple textural observations (Chen & El Goresy 2000), especially of radial cracks in the minerals surrounding the glasses. These cracks are generated by the expansion related to decompression of the dense glass that formed by shock-induced melting and quenching at high pressure (**Figure 14**). The observation of decompression cracks, combined with other arguments,

has been used to rule out the formation of glasses (often termed maskelynite) in Martian meteorites by a pressure-induced amorphization (El Goresy et al. 2013).

Diaplectic glasses are formed experimentally in silicates in a few microseconds, the typical time duration of experimental shocks. For instance, quartz and feldspars transform into diaplectic glasses at shock pressures between 25 and 35 GPa. Similar dense glasses can also be formed by static cold compression at lower pressures within a similar pressure range (Richet & Gillet 1997, Tomioka et al. 2010).

Quartz and feldspars recovered from shock and static experiments show that, before reaching the pressure of complete amorphization, the samples are gradually invaded by PDFs. These PDFs correspond to thin amorphous lamellae that lie along specific crystallographic planes (**Figure 14**) and have the same chemical composition as the host crystal (Langenhorst & Deutsch 1994).

Kubo et al. (2010) recently showed that the amorphization pressure of plagioclase decreases with increasing temperature and that, when temperature is high enough, jadeite grows at the expense of amorphous plagioclase, followed by the nucleation of other minerals such as stishovite or garnet. Under equilibrium conditions, one would expect the formation of an assemblage containing not only jadeite but also stishovite and garnet. Such an observation again shed light on the important role kinetics plays in the formation of high-pressure mineral assemblages during shock events. The breakdown of plagioclase and the sequence of crystallization can thus constrain the (P,T,t) history of a shock event.

SUMMARY POINTS

1. The maximum pressure reached during a shock is controlled by the impact velocity and the nature of the material of both the impactor and the target.
2. The time duration of the shock is related, at the first order, to the size and the relative velocities of the impactor and target.
3. The temperature reached during a shock is heterogeneous. Bulk melting of a rock can be achieved only at very high pressure.
4. During propagation of a shock wave, local heterogeneities (such as pores or cracks) in rocks induce both pressure and temperature spikes that relax on different timescales: a few nanoseconds to microseconds for pressure, and a fraction of a second for temperature.
5. Shear melt veins and melt pockets that result from these temperature spikes and local strains are unique zones where the temperature is high enough to induce the formation of high-pressure minerals. These minerals constrain the shock pressure more reliably than does the classical scale based on the comparison of defect densities or changes in refractive indices.
6. Phase transformations observed in static laboratory experiments, and the corresponding phase diagrams and kinetics laws, can be used to estimate the time duration of a shock.

FUTURE ISSUES

1. Only a few of the known high-pressure phases have been discovered in terrestrial impacts, in stark contrast with the multitude of high-pressure phases identified in meteorites. A search for new high-pressure minerals in terrestrial impacts is warranted.

2. Electron microscopy and focused ion beams may be used more generally to unravel the mineralogy of shocked rocks at the nanoscale. Each tiny mineral reflects part of the (P,T,t) history of the shock.
3. Mineralogy and petrology should be introduced into numerical models of crater formation to enable forward prediction of the (P,T) metamorphic maps of crater rocks and ejecta blankets.
4. The crustal structure of planetary bodies (such as Vesta, Mars, and the Moon) may be probed through the petrology and localization of the rocks of ejecta blankets.
5. Shock experiments should be performed on synthetic nanorocks, in which the typical mineral size is on the order of a few tens of nanometers.
6. High-performance computers can be used to study, through molecular dynamics or other means, the physics of wave propagation in heterogeneous media at a scale of a few nanometers to a few micrometers.

DISCLOSURE STATEMENT

The authors are not aware of any affiliations, memberships, funding, or financial holdings that might be perceived as affecting the objectivity of this review.

ACKNOWLEDGMENTS

The authors wish to kindly acknowledge the following persons: T. Ferroir, for his input during the writing of the paper; J. Badro, S. Dorfman, and S. Escrig, who carefully read the manuscript through the eyes of potential readers; F. Guyot and A. Meibom, who made valuable comments on an earlier version of the article; and G.S. Collins, who kindly authorized the use of one of his figures. We thank P. Vonlanthen for providing SEM images of the lunar meteorite presented in this article. Finally, we wish to warmly thank our colleagues M. Miyahara and E. Ohtani for their ongoing help and their enthusiasm for the study of shocked meteorites.

LITERATURE CITED

Albarede F. 2009. Volatile accretion history of the terrestrial planets and dynamic implications. *Nature* 461:1227–33

Barrat JA, Gillet P, Sautter V, Jambon A, Javoy M, et al. 2002. Petrology and geochemistry of the basaltic shergottite North West Africa 480. *Meteorit. Planet. Sci.* 37:487–99

Beck P, Ferroir T, Gillet P. 2007. Shock-induced compaction, melting, and entrapment of atmospheric gases in Martian meteorites. *Geophys. Res. Lett.* 34:L01203

Beck P, Gillet P, El Goresy A, Mostefaoui S. 2005. Timescales of shock processes in the solar system from mineralogical transformations in chondrites and Martian meteorites. *Nature* 435:1071–74

Beck P, Gillet P, Gautron L, Daniel I, El Goresy A. 2004. A new natural high-pressure (Na, Ca)-hexaluminosilicate [$(Ca_xNa_{1-x})Al_{3+x}Si_{3-x}O_{11}$] in shocked Martian meteorites. *Earth Planet. Sci. Lett.* 219:1–12

Benzerara K, Guyot F, Barrat JA, Gillet P, Lesourd M. 2002. Cristobalite inclusions in the Tatahouine achondrite: implications for shock conditions. *Am. Mineral.* 87:1250–56

Binns RA. 1970. $(Mg,Fe)_2SiO_4$ spinel in a meteorite. *Phys. Earth Planet. Inter.* 3:156–60

Biren MB, Spray JG. 2011. Shock veins in the central uplift of the Manicouagan impact structure: context and genesis. *Earth Planet. Sci. Lett.* 303:310–22

Blase X, Gillet P, San Miguel A, Mélinon P. 2004. Exceptional ideal strength of carbon clathrates. *Phys. Rev. Lett.* 92:215505–9

Bogard DD, Johnson P. 1983. Martian gas in an Antarctic meteorite. *Science* 221:651–54
Bottke WF, Vokrouhlicky D, Minton D, Nesvorny D, Morbidelli A, et al. 2012. An Archaean heavy bombardment from a destabilized extension of the asteroid belt. *Nature* 485:78–81
Canup RM, Asphaug E. 2001. Origin of the Moon in a giant impact near the end of the Earth's formation. *Nature* 412:708–12
Chao ECT, Fahey JJ, Littler J, Milton DJ. 1962. Stishovite, SiO_2, a very high pressure new mineral from Meteor Crater, Arizona. *J. Geophys. Res.* 67:419–421
Chen M, El Goresy A. 2000. The nature of maskelynite in shocked meteorites: not diaplectic glass but a glass quenched from shock-induced dense melt at high pressures. *Earth Planet. Sci. Lett.* 179:489–502
Chen M, Sharp TG, El Goresy A, Wopenka B, Xie X. 1996. The majorite-pyrope +magnesiowüstite assemblage: constraints on the history of shock veins in chondrites. *Science* 271:1570–73
Chen M, Shu J, Mao HK, Xie X, Hemley RJ. 2003. Natural occurrence and synthesis of two new post-spinel polymorphs of chromite. *Proc. Natl. Acad. Sci. USA* 100:14651–54
Chyba CF, Thomas PJ, Zahnle KJ. 1993. The 1908 Tunguska explosion: atmospheric disruption of a stony asteroid. *Nature* 361:40–44
Coes L. 1953. A new dense crystalline silica. *Science* 118:131–32
Collins GS, Melosh HJ, Marcus RA. 2005. Earth Impact Effects Program: a Web-based computer program for calculating the regional environmental consequences of a meteoroid impact on Earth. *Meteorit. Planet. Sci.* 40:817–40
Collins GS, Melosh HJ, Osinski GR. 2012. The impact-cratering process. *Elements* 8:25–30
El Goresy A, Chen M, Dubrovinsky L, Gillet P, Graup G. 2001a. An ultradense polymorph of rutile with seven-coordinated titanium from the Ries crater. *Science* 293:1467–70
El Goresy A, Chen M, Gillet P, Dubrovinsky L, Graup G, Ahuja R. 2001b. A natural shock-induced dense polymorph of rutile with α-PbO_2 structure in the suevite from the Ries crater in Germany. *Earth Planet. Sci. Lett.* 192:485–95
El Goresy A, Dubrovinsky L, Gillet P, Mostefaoui S, Graup G, et al. 2003. A new natural, super-hard, transparent polymorph of carbon from the Popigai impact crater, Russia. *C. R. Geosci.* 335:889–98
El Goresy A, Gillet P, Chen M, Künstler F, Graup G, Stähl V. 2001c. In situ discovery of shock-induced graphite-diamond phase transition in gneisses from the Ries Crater, Germany. *Am. Mineral.* 86:611–21
El Goresy A, Gillet P, Miyahara M, Ohtani E, Ozawa S, et al. 2013. Shock-induced deformation of Shergottites: shock-pressures and perturbations of magmatic ages on Mars. *Geochim. Cosmochim. Acta* 101:233–62
Elkins-Tanton LT. 2012. Magma oceans in the inner solar system. *Annu. Rev. Earth Planet. Sci.* 40:113–39
Ferroir T, Beck P, Van de Moortele B, Bohn M, Reynard B, et al. 2008. Akimotoite in the Tenham meteorite: crystal chemistry and high-pressure transformation mechanisms. *Earth Planet. Sci. Lett.* 275:26–31
Ferroir T, Dubrovinsky L, El Goresy A, Simionovici A, Nakamura T, Gillet P. 2010. Carbon polymorphism in shocked meteorites: evidence for new natural ultrahard phases. *Earth Planet. Sci. Lett.* 290:150–54
Fiquet G, Auzende AL, Siebert J, Corgne A, Bureau H, et al. 2010. Melting of peridotite to 140 gigapascals. *Science* 329:1516–18
French BM. 1998. *Traces of Catastrophe: A Handbook of Shock-Metamorphic Effects in Terrestrial Meteorite Impact Structures.* LPI Contribution No. 954. Houston: Lunar and Planetary Institute. 120 pp.
French BM, Koeberl C. 2010. The convincing identification of terrestrial meteorite impact structures: what works, what doesn't, and why. *Earth-Sci. Rev.* 98:123–70
Gillet P, Chen C, Dubrovinsky L, Goresi E. 2000. Natural $NaAlSi_3O_8$-hollandite in the shocked Sixiangkou meteorite. *Science* 287:1633–36
Gillet P, El Goresy A, Beck P, Chen M. 2007. High-pressure mineral assemblages in shocked meteorites and shocked terrestrial rocks: mechanisms of phase transformations and constraints to pressure and temperature histories. *Geol. Soc. Am. Spec. Pap.* 421:57–82
Hartmann WK. 2002. Mars cratering chronology system: improved isochrons and dates. *Meteorit. Planet. Sci.* 37:A60
Heider N, Kenkmann T. 2003. Numerical simulation of temperature effects at fissures due to shock loading. *Meteorit. Planet. Sci.* 38:1451–60
Housen KR, Holsapple KA. 2011. Ejecta from impact craters. *Icarus* 211:856–75

Ivanov BA. 2005. Numerical modeling of the largest terrestrial meteorite craters. *Solar Syst. Res.* 39:381–409
Jacobsen SB. 2005. The Hf-W isotopic system and the origin of the Earth and Moon. *Annu. Rev. Earth Planet. Sci.* 33:531–70
Johnson BC, Melosh HJ. 2012. Impact spherules as a record of an ancient heavy bombardment of Earth. *Nature* 485:75–77
Jones AP, Price GD, Price NJ, DeCarli PS, Clegg RA. 2002. Impact induced melting and the development of large igneous provinces. *Earth Planet. Sci. Lett.* 202:551–61
Jourdan F, Reirnold WU, Deutsch A. 2012. Dating terrestrial impact structures. *Elements* 8:49–53
Jutzi M, Benz W, Michel P. 2008. Numerical simulations of impacts involving porous bodies: I. Implementing sub-resolution porosity in a 3D SPH hydrocode. *Icarus* 198:242–55
Jutzi M, Michel P, Hiraoka K, Nakamura AM, Benz W. 2009. Numerical simulations of impacts involving porous bodies: II. Comparison with laboratory experiments. *Icarus* 201:802–13
Kerschhofer L, Rubie DC, Sharp TG, McConnell JDC, Dupas-Bruzek C. 2000. Kinetics of intracrystalline olivine-ringwoodite transformation. *Phys. Earth Planet. Inter.* 121:59–76
Kerschhofer L, Sharp TG, Rubie DC. 1996. Intracrystalline transformation of olivine to wadsleyite and ringwoodite under subduction zone conditions. *Science* 274:79–81
Kieffer SW, Phakey PP, Christie JM. 1976. Shock processes in porous quartzite: transmission electron microscope observations and theory. *Contrib. Mineral. Petrol.* 59:41–93
Kubo T, Kimura M, Kato T, Nishi M, Tominaga A, et al. 2010. Plagioclase breakdown as an indicator for shock conditions of meteorites. *Nat. Geosci.* 3:41–45
Lakshtanov DL, Sinogeikin SV, Litasov KD, Prakapenka VB, Hellwig H, et al. 2007. The post-stishovite phase transition in hydrous alumina-bearing SiO_2 in the lower mantle of the earth. *Proc. Natl. Acad. Sci. USA* 104:13588–90
Langenhorst F, Deutsch A. 1994. Shock experiments on pre-heated α- and β-quartz: I. Optical and density data. *Earth Planet. Sci. Lett.* 125:407–20
Langenhorst F, Deutsch A. 2012. Shock metamorphism of minerals. *Elements* 8:31–36
Langenhorst F, Dressler B. 2003. First observation of silicate hollandite in a terrestrial rock. *Proc. 3rd Int. Conf. Large Meteor. Impacts, Nördlingen, Ger., Aug. 5–7*, Abstr. 4046
Langenhorst F, Hornemann U. 2005. Shock experiments on minerals: basic physics and techniques. In *EMU Notes in Mineralogy*. Vol. 7: *Mineral Behaviour at Extreme Conditions*, ed. R Miletich, pp. 357–87. Heidelberg, Ger.: Eur. Mineral. Soc.
Langenhorst F, Poirier JP. 2000a. Anatomy of black veins in Zagami: clues to the formation of high-pressure phases. *Earth Planet. Sci. Lett.* 184:37–55
Langenhorst F, Poirier JP. 2000b. 'Eclogitic' minerals in a shocked basaltic meteorite. *Earth Planet. Sci. Lett.* 176:259–65
Li Q, Ma YM, Oganov AR, Wang HB, Wang H, et al. 2009. Superhard monoclinic polymorph of carbon. *Phys. Rev. Lett.* 102:175506
Mader CL. 1965. Initiation of detonation by interaction of shocks with density discontinuities. *Phys. Fluids* 8:1811–16
Mao WL, Mao HK, Eng PJ, Trainor TP, Newville M, et al. 2003. Bonding changes in compressed superhard graphite. *Science* 302:425–27
Marchi S, McSween HY, O'Brien DP, Schenk P, De Sanctis MC, et al. 2012. The violent collisional history of asteroid 4 Vesta. *Science* 336:690–94
Masaitis VL, Futergendler SI, Gnevyshev MA. 1972. The diamonds in the Popigai meteoritic crater. *Zap. Vses. Mineral. Obshch.* 101:108–13
Melosh HJ, ed. 1989. *Impact Cratering: A Geologic Process*. New York: Oxford Univ. Press. 245 pp.
Melosh HJ. 2005. The mechanics of pseudotachylite formation. In *Impact Tectonics*, ed. C Koeberl, H Henkel, pp. 55–80. Berlin: Springer
Mishima O, Calvert LD, Whalley E. 1984. 'Melting ice' I at 77 K and 10 kbar: a new method of making amorphous solids. *Nature* 310:393–94
Miyahara M, El Goresy A, Ohtani E, Nagase T, Nishijima M, et al. 2008. Evidence for fractional crystallization of wadsleyite and ringwoodite from olivine melts in chondrules entrained in shock-melt veins. *Proc. Natl. Acad. Sci. USA* 105:8542–47

Miyahara M, Ohtani E, Kimura M, El Goresy A, Ozawa S, et al. 2010. Coherent and subsequent incoherent ringwoodite growth in olivine of shocked L6 chondrites. *Earth Planet. Sci. Lett.* 295:321–27

Miyahara M, Ohtani E, Ozawa S, Kimura M, El Goresy A, et al. 2011. Natural dissociation of olivine to (Mg,Fe)SiO_3 perovskite and magnesiowüstite in a shocked Martian meteorite. *Proc. Natl. Acad. Sci. USA* 108:5999–6003

Montmerle T, Augereau JC, Chaussidon M, Gounelle M, Marty B, Morbidelli A. 2006. Solar system formation and early evolution: the first 100 million years. *Earth Moon Planets* 98:39–95

Morbidelli A, Lunine JI, O'Brien DP, Raymond SN, Walsh KJ. 2012. Building terrestrial planets. *Annu. Rev. Earth Planet. Sci.* 40:251–75

Mosenfelder JL, Asimow PD, Ahrens TJ. 2007. Thermodynamic properties of Mg_2SiO_4 liquid at ultra-high pressures from shock measurements to 200 GPa on forsterite and wadsleyite. *J. Geophys. Res.* 112:B06208

Mosenfelder JL, Marton FC, Ross CR, Kerschhofer L, Rubie DC. 2001. Experimental constraints on the depth of olivine metastability in subducting lithosphere. *Phys. Earth Planet. Inter.* 127:165–80

Nakamuta Y, Aoki Y. 2000. Mineralogical evidence for the origin of diamond in ureilites. *Meteorit. Planet. Sci.* 35:487–93

Ohtani E, Kimura Y, Kimura M, Takata T, Kondo T, Kubo T. 2004. Formation of high-pressure minerals in shocked L6 chondrite Yamato 791384: constraints on shock conditions and parent body size. *Earth Planet. Sci. Lett.* 227:505–15

Ohtani E, Ozawa S, Miyahara M, Ito Y, Mikouchi T, et al. 2011. Coesite and stishovite in a shocked lunar meteorite, Asuka-881757, and impact events in lunar surface. *Proc. Natl. Acad. Sci. USA* 108:463–66

Pierazzo E, Artemieva N. 2012. Local and global environmental effects of impacts on Earth. *Elements* 8:55–60

Price GD, Putnis A, Agrell SO. 1979. Electron petrography of shock-produced veins in the Tenham chondrite. *Contrib. Mineral. Petrol.* 71:211–18

Reimold WU, Jourdan F. 2012. Impact! Bolides, craters, and catastrophes. *Elements* 8:19–24

Richet P, Gillet P. 1997. Pressure-induced amorphization of minerals: a review. *Eur. J. Mineral.* 9:907–33

Rost R, Dolgov YA, Vishnevsky SA. 1978. Gases in inclusions of impact glass in the Ries Crater, West Germany, and finds of high-pressure carbon polymorphs. *Dokl. Akad. Nauk SSSR* 241:695–98

Sharp TG, DeCarli PS. 2006. Shock effects in meteorites. In *Meteorites and the Early Solar System II*, ed. DS Lauretta, HY McSween, pp. 653–77. Tucson: Univ. Ariz. Press

Sharp TG, El Goresy A, Wopenka B, Chen M. 1999. A post-stishovite polymorph in the meteorite shergotty. *Science* 284:1511–13

Sharp TG, Lingemann CM, Dupas C, Stöffler D. 1997. Natural occurrences of $MgSiO_3$-ilmenite and evidence for $MgSiO_3$-perovskite in a shocked L chondrite. *Science* 277:352–55

Spray JG. 2010. Frictional melting processes in planetary materials: from hypervelocity impact to earthquakes. *Annu. Rev. Earth Planet. Sci.* 38:221–54

Stahle V, Altherr R, Koch M, Nasdala L. 2008. Shock-induced growth and metastability of stishovite and coesite in lithic clasts from suevite of the Ries impact crater (Germany). *Contrib. Mineral. Petrol.* 155:457–72

Stahle V, Altherr R, Nasdala L, Ludwig T. 2011. Ca-rich majorite derived from high-temperature melt and thermally stressed hornblende in shock veins of crustal rocks from the Ries impact crater (Germany). *Contrib. Mineral. Petrol.* 161:275–91

Stishov SM. 1963. Equilibrium line between coesite and rutile-like modification of silicon. *Dokl. Akad. Nauk SSSR* 148:1186

Stöffler D, Bischoff A, Buchwald V, Rubin AE. 1988. Shock effects in meteorites. In *Meteorites and the Early Solar System*, ed. JF Kerridge, MS Matthews, pp. 165–202. Tucson: Univ. Ariz. Press

Stöffler D, Keil K, Scott ERD. 1991. Shock metamorphism of ordinary chondrites. *Geochim. Cosmochim. Acta* 55:3845–67

Stöffler D, Langenhorst F. 1994. Shock metamorphism of quartz in nature and experiment: I. Basic observation and theory. *Meteoritics* 29:155–81

Stöffler D, Ryder G, Ivanov BA, Artemieva NA, Cintala MJ, Grieve RAF. 2006. Cratering history and lunar chronology. *Rev. Mineral. Geochem.* 60:519–96

Strom RG, Malhotra R, Ito T, Yoshida F, Kring DA. 2005. The origin of planetary impactors in the inner solar system. *Science* 309:1847–50

Tomioka N, Fujino K. 1997. Natural (Mg,Fe)SiO_3-ilmenite and -perovskite in the Tenham meteorite. *Science* 277:1084–86

Tomioka N, Kondo H, Kunikata A, Nagai T. 2010. Pressure-induced amorphization of albitic plagioclase in an externally heated diamond anvil cell. *Geophys. Res. Lett.* 37:L21301

Treiman AH, Gleason JD, Bogard DD. 2000. The SNC meteorites are from Mars. *Planet. Space Sci.* 48:1213–320

Van de Moortele B, Reynard B, McMillan PF, Wilson M, Beck P, et al. 2007a. Shock-induced transformation of olivine to a new metastable $(Mg,Fe)_2SiO_4$ polymorph in Martian meteorites. *Earth Planet. Sci. Lett.* 261:469–75

Van de Moortele B, Reynard B, Rochette P, Jackson M, Beck P, et al. 2007b. Shock-induced metallic iron nanoparticles in olivine-rich Martian meteorites. *Earth Planet. Sci. Lett.* 262: 37–49

Warren PH, Ulff-Møller F, Kallemeyn GW. 2005. "New" lunar meteorites: impact melt and regolith breccias and large-scale heterogeneities of the upper lunar crust. *Meteorit. Planet. Sci.* 40:989–1014

Wunnemann K, Collins GS, Osinski GR. 2008. Numerical modelling of impact melt production in porous rocks. *Earth Planet. Sci. Lett.* 269:529–38

Xie X, Minitti ME, Chen M, Mao HK, Wang D, et al. 2002. Natural high-pressure polymorph of merrillite in the shock veins of the Suizhou meteorite. *Geochim. Cosmochim. Acta* 66:2439–44

Xie X, Sharp TG. 2003. TEM observations of amorphized silicate-perovskite, akimotoite and Ca-rich majorite in a shock-induced melt vein in the Tenham L6 chondrite. *34th Annu. Lunar Planet. Sci. Conf., League City, Tex., Mar. 17–21*, Abstr. 1469

Xie Z, Sharp TG, DeCarli PS. 2006. High-pressure phases in a shock-induced melt vein of the Tenham meteorite: constraints on shock pressure and duration. *Geochim. Cosmochim. Acta* 70:504–15

Annual Review
of Earth and
Planetary Sciences
Volume 41, 2013

Contents